Supporting information for:

# Role of $SiO_2$ in Enhancing CO Yield by Using Silica-supported $La_{0.5}Ba_{0.5}FeO_3$ in Reverse Water-gas Shift Chemical Looping

Hanzhong Shi, Jiawei Guo, Prabhsimran Singh, Venkat R. Bhethanabotla, John N. Kuhn

Department of Chemical, Biological, and Materials Engineering, University of South Florida

Tampa, Florida 33620, United States of America

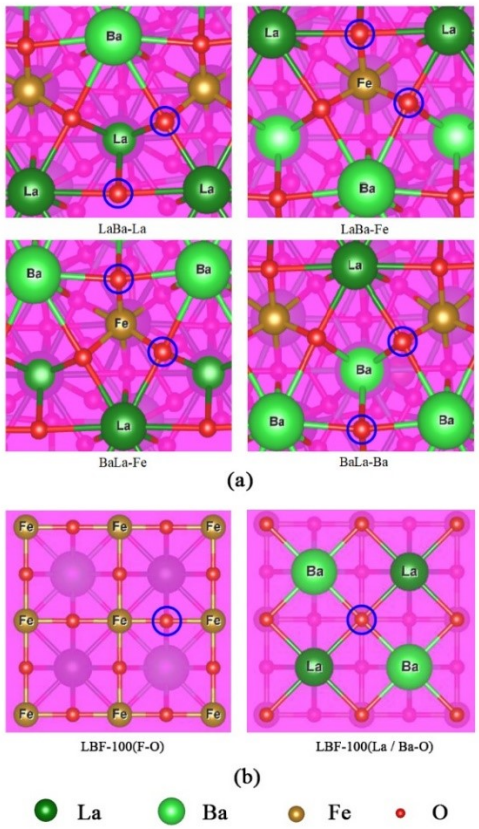


**Figure S1.** Detailed surface constructions of (a) LBF-111, and (b) LBF-100. The blue circle highlighted the possible sites to form oxygen vacancy.

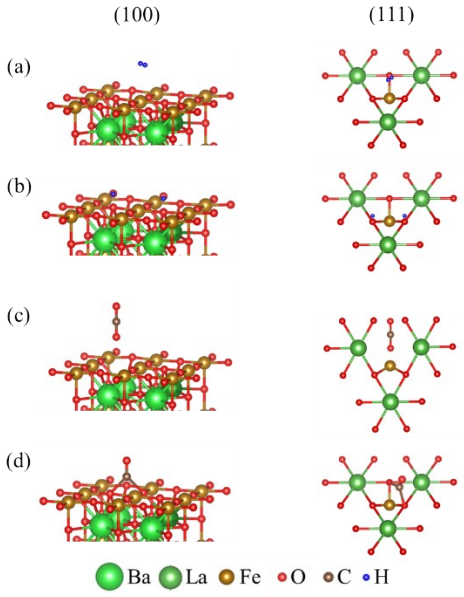


**Figure S2.** Surface construction of (a) $H_2$-physisorption, (b) Chemisorption of dissociated $H_2$, (c) $CO_2$-physisorption, and (d) CO-chemisorption. Left column is the adsorptions on LBF-111(Fe-O). Right column is the adsorptions on LBF-111(BaLa-Fe).

**S1 Computational methods**

The DFT calculations in this study were performed using Quantum ESPRESSO software (version 6.2.1) [1, 2]. The materials models used in the calculations are referenced from the materials project database, with corresponding index numbers [3]. The plane wave basis set and gradient generalization approximation for electron densities were used [4, 5]. The projector augmented wave (PAW) potentials and Perdew-Burke-Ernzerhof (PBE) variant of exchange-correlation functional were employed [6, 7]. In this study, the energy convergence criterion was set to $10^{-6}$ eV per atom, and the force convergence criterion was set to 0.005 eV/Å. A constant cutoff of 40 Ry (544 eV) was selected. A k-point mesh of (4 × 4 × 1) was used for the Brillouin zone sampling. The Hubbard U correction was not applied in this calculation, as the trend of energies did not show a significant shift with or without the application of the Hubbard U correction [8, 9].

**S1.1 Oxygen vacancy formation energy calculations**

X-ray diffraction (XRD) results showed a shift in the (111) plane when $SiO_2$ was added as the support material. Therefore, the LBF structure with an exposed (111) plane (LBF-111) was the focus of this study, while LBF with an exposed (100) plane (LBF-100) was selected as the comparison structure. One 60-atom supercell of LBF-111 (Figure S3(a)) and two 60-atom supercells of LBF-100 (Figure S3(b) and (c)) were constructed using VESTA (Visualization for Electronic and Structural Analysis, Ver. 3). An 18 Å vacuum was added on top of each structure to create a slab. To introduce oxygen vacancies, one oxygen atom was removed from the top surface of each supercell.

The extent of oxygen vacancy (δ) is defined as the oxygen deficiency per unit cell. To form the surface slab with oxygen vacancy, one oxygen atom was removed from the (111) or (100) plane. Then, the oxygen vacancy formation energy ($E_{Ovac}$) was calculated by Eq. S1.

$$E_{O_{vac}} = E_{S_{Ovac}} - \delta \times \frac{n}{2} E_{O_2} - E_S \qquad (S1)$$

where $E_{O_{vac}}$ is the oxygen vacancy formation energy. $E_{S_{Ovac}}$ is the total energy of the perovskite supercell with oxygen vacancy. $E_{O_2}$ is the molecular energy of oxygen. $E_S$ is the total energy of the pure stoichiometric perovskite supercell. $n$ is the number of unit cells. $\delta$ is the extent of oxygen vacancy.

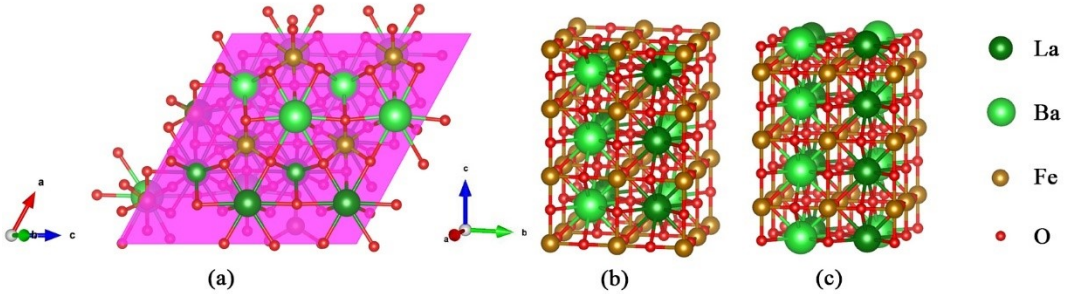


**Figure S3.** Supercells of (a) (111) exposed LBF where (111) plane is marked to pink, (b) (100) exposed LBF with Fe layer on the top, and (c) (100) exposed LBF with La and Ba on the top.

**S1.2 $H_2$, CO, and $CO_2$ adsorption energy calculations**

The stoichiometric perovskite surface was utilized for the calculations for $H_2$ and CO adsorption energies. For $CO_2$ adsorption energy calculations, the surface utilized was the reduced perovskites with oxygen vacancy, where the oxygen vacancy is the kay factor for the second step in RWGS-CL reaction (Eq. 1.2) [8]. The initial adsorption distance for $H_2$, CO, and $CO_2$ was set to 1.0 Å from the surface. The adsorption energy of the materials ($E_{adsi}$) is calculated by Eq. S2.

$$E_{adsi} = E_{P+i} - E_i - E_P \qquad (S2)$$

where *i* represents $H_2$, CO, or $CO_2$, $E_P$ is the energy of either the pure or oxygen vacant perovskite, $E_{P+i}$ is the energy of the combined system of *i* adsorbed on the perovskite, $E_i$ is the energy of $H_2$, CO, or $CO_2$.

**S1.3 Vibrational frequency calculations for adsorbed $CO_2$**

For each oxygen vacated supercell with adsorbed $CO_2$, the atoms in $CO_2$ were nudged by δb (along the b-direction) or δc (along the c-direction) with a selected nudged distance of 0.11 Å. The nudged distance of 0.11 Å was determined after performing simulations with distances ranging from 0.05 to 0.20 Å. The energy of each nudged structure was calculated using Quantum ESPRESSO, and the vibrational frequency was calculated from a 6×6 Hessian matrix [10].

**S2 Experimental procedures**

X-ray diffraction (XRD) was performed to confirm the crystal structure of LBF and LBF/$SiO_2$ samples by a Bruker X-ray Diffractometer. X-ray fluorescence (XRF; Bruker, PUMA S2) was used for testing the bulk element compositions of the samples. X-ray photoelectron spectroscopy (XPS, Physical Electronics 5400) was used for measuring the near surface binding energy of LBF and LBF/$SiO_2$. $CO_2$ chemisorption experiments (Quantachrome Autosorb IQ) were used for testing the amount of chemisorbed $CO_2$. $CO_2$ adsorption of reduced LBF and LBF/$SiO_2$ were calculated by extrapolation method based on the isotherms obtained by measuring the volume of $CO_2$ adsorbed at a set of partial pressure (P / Po) at 298 K[11, 12]. The intercept represents the volume of $CO_2$ chemisorption amount that could be found from the regression of near flat points in the isotherms. Then, Eq. S3 is used to calculate the amount of $CO_2$ chemisorption on perovskite site, where $S_{CO2,i}$ (μmol/$g_{LBF}$) is CO chemisorption amount on perovskite site for LBF or LBF/SiO, $v_{CO2,i}$ ($cm^3$/g) is the volume of $CO_2$ absorbed on LBF or LBF/$SiO_2$, A is the conversion number (44.64 μmol/$cm^3$), $x_i$ is the perovskite concentration in LBF (100wt%) or LBF/$SiO_2$ (25wt%).

$$S_{CO_2,i} = \frac{Av_{CO_2,i}}{x_i} \quad (Eq.\ S3)$$

The FT-IR spectrometer (Thermo Scientific, Nicolet iS50) with a high-temperature reaction chamber (Harrick, HVC-DPR-5) was used for the DRIFTS experiments of temperature-programmed desorption with $CO_2$ (DRIFTS-TPD-$CO_2$). A gas manifold consisting of a set of mass flow controllers (Alicat) was used to supply the following gases for the experiments, Ar (Airgas, ultra-high purity), $H_2$ (Airgas, ultra-high purity), and $CO_2$ (Airgas, industrial grade).

For TPO experiments, a U-shape reactor (ID = 0.4 cm) was connected to a gas manifold consisting of a set of mass flow controllers (Alicat). A total gas flow rate of 50 sccm in used in this study. A water bubbler purged by He is used for flowing $H_2O$ into reactor. A mass of approximately 75 mg LBF or LBF/$SiO_2$ was placed into the reactor between quartz wool plugs. The sample was reduced under 10% $H_2$ / He at 500°C for 30 min. Then cold the reactor to room temperature. Following the oxidation experiments were performed under different oxidizers (2.5% $O_2$ / He, 10% $CO_2$ / He, and 10% $H_2O$ / He) heated by the furnace from room temperature to 800°C (heating rate of 10°C/min). The reactor effluent was analyzed by a mass spectrometer (MS; MKS, Cirrus 3).

**Data availability**

All data used in this paper is available. The data in Table 1 is from previous published paper [13, 14].

**Reference**

1. P. Giannozzi, O. Andreussi, T. Brumme, O. Bunau, M. Buongiorno Nardelli, M. Calandra, R. Car, C. Cavazzoni, D. Ceresoli, M. Cococcioni, N. Colonna, I. Carnimeo, A. Dal Corso, S. de Gironcoli, P. Delugas, R. A. DiStasio, A. Ferretti, A. Floris, G. Fratesi, G. Fugallo, R. Gebauer, U. Gerstmann, F. Giustino, T. Gorni, J. Jia, M. Kawamura, H. Y. Ko, A. Kokalj, E. Küçükbenli, M. Lazzeri, M. Marsili, N. Marzari, F. Mauri, N. L. Nguyen, H. V. Nguyen, A. Otero-de-la-Roza, L. Paulatto, S. Poncé, D. Rocca, R. Sabatini, B. Santra, M. Schlipf, A. P. Seitsonen, A. Smogunov, I. Timrov, T. Thonhauser, P. Umari, N. Vast, X. Wu and S. Baroni, *Journal of Physics: Condensed Matter*, 2017,

**29**, 465901.
2. K. Burke, *The Journal of Chemical Physics*, 2012, **136**, 150901.
3. A. Jain, S. P. Ong, G. Hautier, W. Chen, W. D. Richards, S. Dacek, S. Cholia, D. Gunter, D. Skinner, G. Ceder and K. A. Persson, 2013, **1**, 011002.
4. P. Giannozzi, S. Baroni, N. Bonini, M. Calandra, R. Car, C. Cavazzoni, D. Ceresoli, G. L. Chiarotti, M. Cococcioni, I. Dabo, A. Dal Corso, S. de Gironcoli, S. Fabris, G. Fratesi, R. Gebauer, U. Gerstmann, C. Gougoussis, A. Kokalj, M. Lazzeri, L. Martin-Samos, N. Marzari, F. Mauri, R. Mazzarello, S. Paolini, A. Pasquarello, L. Paulatto, C. Sbraccia, S. Scandolo, G. Sclauzero, A. P. Seitsonen, A. Smogunov, P. Umari and R. M. Wentzcovitch, *J. Phys.: Condens. Matter*, 2009, **21**, 395502.
5. K. F. Garrity, J. W. Bennett, K. M. Rabe and D. Vanderbilt, *Computational Materials Science*, 2014, **81**, 446-452.
6. G. Kresse and D. Joubert, *Physical Review B*, 1999, **59**, 1758-1775.
7. J. P. Perdew, K. Burke and M. Ernzerhof, *Physical Review Letters*, 1996, **77**, 3865-3868.
8. D. Maiti, Y. A. Daza, M. M. Yung, J. N. Kuhn and V. R. Bhethanabotla, *Journal of Materials Chemistry A*, 2016, **4**, 5137-5148.
9. I. W. Boateng, R. Tia, E. Adei, N. Y. Dzade, C. R. A. Catlow and N. H. de Leeuw, *PCCP*, 2017, **19**, 7399-7409.
10. D. S. Sholl and J. A. Steckel, *Density functional theory: a practical introduction*, John Wiley & Sons, 2011.
11. S. Brunauer, P. H. Emmett and E. Teller, *Journal of the American chemical society*, 1938, **60**, 309-319.
12. C. Chen and W.-S. Ahn, *Chemical Engineering Journal*, 2011, **166**, 646-651.
13. H. Shi, V. R. Bhethanabotla and J. N. Kuhn, *Journal of CO2 Utilization*, 2021, **51**, 101638.
14. H. Shi, V. R. Bhethanabotla and J. N. Kuhn, *Journal of Industrial and Engineering Chemistry*, 2023, **118**, 44-52.